Mount Kenya Global Atmosphere Watch Station (MKN): Installation and Meteorological Characterization

STEPHAN HENNE

Swiss Federal Institute for Materials Science and Technology (Empa), Dübendorf, Switzerland

WOLFGANG JUNKERMANN

Forschungszentrum Karlsruhe, Institut für Meteorologie und Klimaforschung IFU, Garmisch-Partenkirchen, Germany

JOSIAH M. KARIUKI AND JOHN ASEYO

Kenya Meteorological Department, Nairobi, Kenya

JÖRG KLAUSEN

Swiss Federal Institute for Materials Science and Technology (Empa), Dübendorf, Switzerland

(Manuscript received 19 July 2007, in final form 23 April 2008)

ABSTRACT

The meteorological conditions at the Mount Kenya (station identifier MKN) tropical Global Atmosphere Watch Programme station are described. Like other stations in mountainous terrain, the site experiences thermally induced wind systems that disturb free tropospheric conditions. Therefore, the adequacy of the site for long-term background atmospheric composition measurements needs to be evaluated. Meteorological parameters for the period June 2002–June 2006 were analyzed, focusing on the development of thermally induced wind systems and boundary layer influence. Filters based on the local wind and day–night differences in specific humidity were developed for selection of times representative of undisturbed free tropospheric conditions. In addition, the convective boundary layer depth was evaluated. Throughout the whole year the station is influenced by thermally induced wind systems and the atmospheric boundary layer. The filters distinguished between thermally and synoptically influenced days. Thermally influenced days (86%) dominated. However, maxima in specific humidity were also reached in the afternoon on synoptically influenced days and were attributed to mixing in the convective boundary layer. During nighttime, downslope wind dominated that carries undisturbed free tropospheric air masses. Nevertheless, during 24% of all nights the specific humidity was also elevated, possibly indicating the presence of residual layers. It is recommended that nighttime data only (2100–0400 UTC) be used for analysis of long-term trends of the free tropospheric background while the remaining data can be used to characterize composition and trends of the regional atmospheric boundary layer. Further exclusion of apparent pollution events and residual layer influence should be considered. With these constraints, the Mount Kenya Global Atmosphere Watch site is adequate for the study of trends and budgets of background atmospheric composition.

1. Introduction

In the early 1990s the World Meteorological Organization (WMO)—with funding from the Global Environment Facility of the World Bank—supported the establishment of six new monitoring stations for the Global Atmosphere Watch (GAW) Programme (World Meteorological Organization 2007; http://www.wmo.int/pages/prog/arep/gaw/gaw_home_en.html) to close apparent gaps in the global air composition monitoring network, especially in the tropics (Brenninkmeijer 1996). The locations of the stations were selected to represent primarily background air masses. Special care was taken to avoid local and regional

Corresponding author address: Dr. Stephan Henne, Laboratory for Air Pollution/Environmental Technology, Swiss Federal Institute for Materials Science and Technology (Empa), 8600 Dübendorf, Switzerland.
E-mail: stephan.henne@empa.ch

DOI: 10.1175/2008JAMC1834.1

sources and sinks of important climate-related gases and aerosols. Three of these stations—Mount Waliguan on the Tibetan Plateau in China (e.g., Ma et al. 2002; Wang et al. 2006), Assekrem in the Algerian Sahara, and Mount Kenya in equatorial East Africa—are mountain stations, whereas the others are located close to the ocean. The measurements planned at the newly established GAW sites include relevant climate variables, selected reactive gases, aerosols, and UV radiation (World Meteorological Organization 2007). Detailed considerations for the monitoring program, including siting requirements, state-of-the-art equipment, and data handling and archiving procedures are summarized in the GAW measurement guide (World Meteorological Organization 2001). An intensive quality assurance and control activity was started to guarantee comparable data from the old and new sites, including regular site audits and operator training.

This article describes the site selection and surroundings of a global baseline monitoring station in East Africa, its installation, and first results that characterize the local meteorological conditions. The objectives were to investigate whether the Mount Kenya site fulfills the requirements for a baseline monitoring station, to augment current knowledge of the local meteorological behavior, and to develop filters based on meteorological observations to distinguish between background (baseline) air masses and locally polluted air masses. The study is limited to a meteorological analysis. It is our intention to give other researchers who intend to do measurements at Mount Kenya detailed meteorological information that can be used in campaign planning. The discussion of trace gas concentrations observed at Mount Kenya is the subject of a companion publication (Henne et al. 2008).

2. Background

a. The climate of equatorial East Africa

The climate of equatorial East Africa is dominated by the seasonal displacement of the intertropical convergence zone (ITCZ; e.g., Asnani 1993; Leroux 2001; Slingo et al. 2005). During boreal summer, the ITCZ is situated far to the north over India (15°–20°N) and along the southern coast of the Arabian Peninsula (10°–15°N), resulting in southerly to southeasterly winds over Kenya (Fig. 1). From September onward, the ITCZ starts to retreat southward, followed by a rainy period ("short rains") from mid-October to December over Kenya. Throughout boreal winter, the ITCZ is situated south of the equator (10°–15°S), extending from the northern tip of Madagascar toward southern Tanzania and then northward toward Lake Victoria. As a consequence, East Africa is dominated by the northeasterly monsoon. When the ITCZ starts to progress northward again, it brings a second rainy period from mid-March to the beginning of June to equatorial East Africa ("long rains"). The ITCZ moves farther north, reestablishing the southeast monsoon over East Africa, and the seasonal cycle is completed.

One noteworthy feature of the boreal monsoon circulation is the East African low-level jet (EALLJ; Asnani 1993; Findlater 1969a). It develops from May onward in the southeast trade winds over Madagascar. With the northward transition of the ITCZ, the EALLJ strengthens and extends northward. It is reflected by the East African Highlands and flows parallel to the coast before it blows eastward off the Somali coast (Somali jet). The EALLJ reaches its maximum extent in June/July when it stretches into India (Fig. 1). The jet maximum generally occurs between 1.0 and 1.6 km above mean sea level (MSL). Wind speed maxima are usually about 20 m s^{-1}, but wind speeds of up to 50 m s^{-1} have been reported (Asnani 1993). Its counterpart blowing from the north along the East African coast during boreal winter is less pronounced.

Much like the whole globe, Africa has experienced rising temperatures in the twentieth century at a rate of about 0.5°C $(100\ yr)^{-1}$ (Hulme et al. 2001). Future predictions for temperature increase in East Africa range from 1.2 to 4.3°C until 2080 in comparison with the period 1961–90. Precipitation is expected to increase in the boreal winter but is expected to decrease in boreal summer, although this prediction is less certain than the temperature projection (Hulme et al. 2001). The Mount Kenya area is the main water reservoir for Kenya. Monitoring the expected changes in climate is thus a basic societal requirement and has an impact on the understanding of climate change for the whole of East Africa.

b. Site evaluation

Several possible sites in Kenya were evaluated during the Mount Kenya feasibility study (Schnell 1978b) comprising several field campaigns from September 1976 to July 1978. Kenya was selected for its political stability and its location on the equator. Measurements of condensation nuclei (CN), carbon dioxide (CO_2), and meteorological conditions were conducted at various sites at Mount Kenya (a total of seven different sites at three different altitudes and on each side of the summit), Mount Kulal (in northwestern Kenya at the southern tip of Lake Turkana), within the Aberdare Range (southwest of Mount Kenya), at Garissa (at 500 m MSL on the coastal plain), and at Watamu (a coastal site

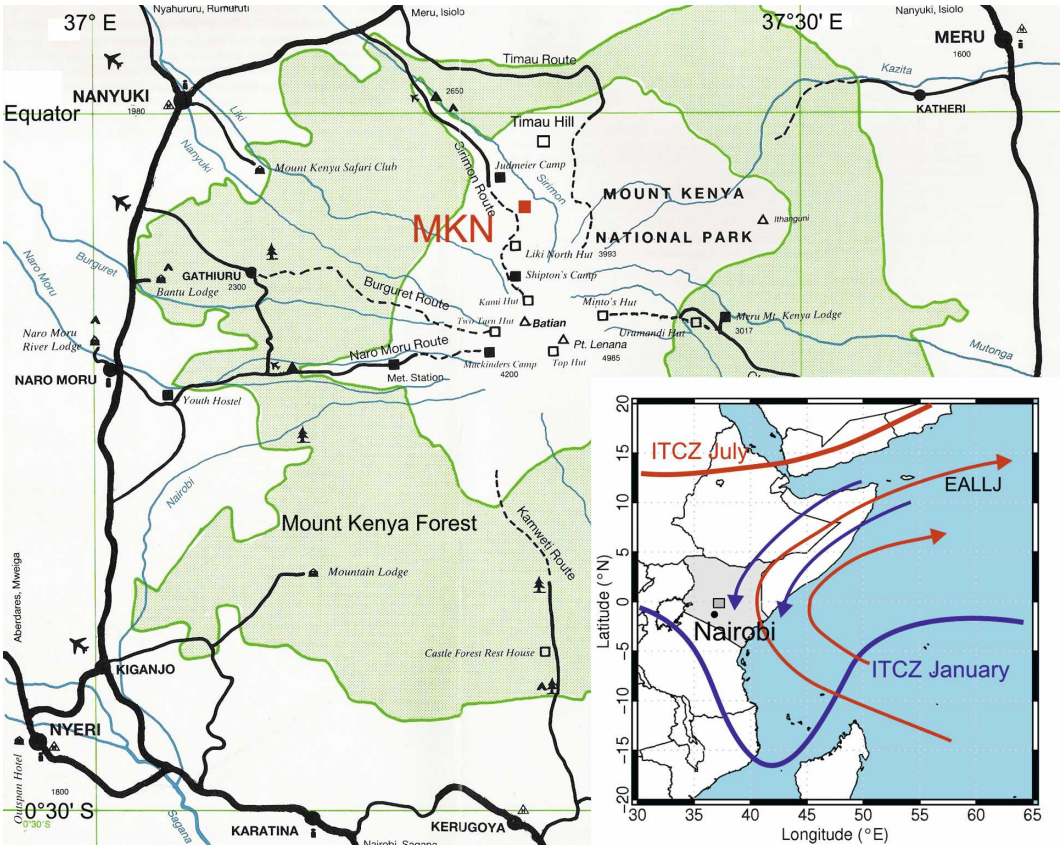

FIG. 1. Map of the Mount Kenya area. The position of the GAW station (MKN) at an elevation of 3680 m MSL is marked by the red square. The green shaded area indicates the forest belt around the mountain. The inset shows the location of Mount Kenya in eastern Africa and the general flow over the western Indian Ocean for the month with the farthest north (south) extent of the ITCZ: July (January). In addition, the approximate position of the EALLJ for July is indicated.

south of Malindi). In addition, several vertical profiles of CN and CO_2 were obtained during a number of aircraft flights. At all mountain sites, the resulting data showed a pronounced diurnal cycle of CO_2 and CN that was also detectable up to a height of 5500 m MSL in the aircraft measurements. Mountain stations are affected by thermally induced up- and downslope wind systems (Whiteman 1990), but during part of the day and during night, free tropospheric conditions often prevail and the sites can be well above the locally influenced atmospheric boundary layer. The study thus concluded that this diurnal cycle would not interfere with the determination of long-term trends.

The location for the construction of the observatory recommended by the feasibility study was on the northern side of Mount Kenya. A site situated west of the Timau route on an isolated hill at 3897 m MSL (Timau Hill) was suggested because CO_2 measurements showed slightly less diurnal variation in comparison with other sites at the same altitude. Sites at higher altitude were discarded because of inadequate accessibility.

c. *Site description*

Subsequent considerations concerning accessibility led to the final positioning (−0.062 °N, 37.297 °E, 3678 m MSL) of the Mount Kenya GAW site (station identifier MKN) on the northwestern slope of Mount Kenya close to the Sirimon route and about 5 km southwest and 200 m below Timau Hill (Fig. 1). Mount Kenya is an isolated, almost conical mountain of volcanic origin, with a diameter of about 60 km, that rises moderately from the surrounding foreland (1800–2000 m MSL) to about 4300 m MSL, where the moderate slopes give way to a jagged alpine landscape. Several rocky peaks, the highest of which is Batian (5199 m MSL), form the mountain top. A number of small valleys run up the sides of the mountain. The foreland surrounding the mountain is mostly used for agriculture (partly irrigated). The mountain itself is surrounded by a forest

FIG. 2. (left) The "river" road (during a rain event) leading up to the (right) station.

zone extending from about 2000 to 2500 m MSL, giving way to bamboo forest, smaller trees, and shrubs. The area has been protected since 1949 as part of the Mount Kenya National Park and was designated a World Heritage Site in 1997. Land use changes are not permitted within the protected area.

The aspect of the northwest-facing slope at the chosen site is 325° (in geography, the aspect generally refers to the direction to which a mountain slope faces). Below the station, grassland (*Festuca pilgrim, Carex* spp.) and shrubs (*Artemisia afra, Protea, Helichrysum*) dominate the vegetation. Some of the shrubs burned down in 1998 and are recovering slowly now. Above the station, grassland and sparse lobelia (*Lobelia telekii, Lobelia keniensis*) are the only vegetation (Fig. 2). The timberline is situated about 5 km to the northwest of and 500 m below the site. The lower edge of the forest is closest in the northward direction at a distance of 11 km. The settlement closest to the station lies near the road connecting Nanyuki and Meru about 17 km northwest and 1500 m below the station (Fig. 1). No major emissions are expected from this settlement besides those resulting from the use of biofuels for cooking purposes. The closest major town, Nanyuki, with a population of 30 000–40 000 (1999 census), is situated farther to the west at a distance of 27 km from the station and at an altitude of 1900 m MSL. Up to the timberline, a dirt road (Sirimon route) leads to the Moyses (Judmeier) camp at 3200 m MSL. Leading up to the final site, the eroded tracks of an abandoned dirt road are still visible. Access to the station with a four-wheel drive car is only possible during dry weather conditions.

The station was designed as a mobile two-container building that was completely equipped and taken into operation in Germany by the Forschungszentrum Karlsruhe (FZK) Institute for Meteorology and Climate Research–Atmospheric Environmental Research and was shipped as a whole unit to Kenya. The containers were shipped directly to Nanyuki at the foot of the mountain in 1998, where they had to be disassembled into manageable pieces and rebuilt at the final location (Fig. 3). The station was officially inaugurated in October 1999. Power to the station is provided by a 26-km overland power line passing through the tropical forest. Other means of power supply were taken into consideration during the planning phase but were discarded because of technical and logistical problems. To set up this power line and to turn it into a reliable power supply was the main factor hampering the operation of the station in the first two years (2000–01) of operation. Intermittent failure of the power line is still the main reason for interruptions in operation. Today, a 10 kilovolt–ampere (kVA) uninterruptable power supply unit provides backup power for about 4 h in case of power outages.

3. Instrumentation and methods

a. Instrumentation

An overview of the instrumentation currently installed at MKN is given in Table 1. The meteorological sensors are installed 1.7 m above the working platform on the station roof and 4.5 m above ground. Wind measurements are taken on a mast 10 m above ground. Data are stored on site with 1-min time resolution on a central datalogger (Vaisala, Inc., MILOS500). Datalogger, trace gas, and aerosol analyzers are installed inside the station. A rain- and snow-protected air inlet system made from glass tubes is mounted at the same height as the meteorological sensors and is connected to a glass manifold (length of 3 m; inner diameter of 5 cm) to which individual instruments inside the container are connected. The manifold is permanently flushed by a

FIG. 3. (left) Reconstruction of the container-based station, and (right) the final station with roof operating platform in January 2000, with the end of the power line and the station transformer in the left of the photograph.

high-volume pump. The container is not air conditioned, and the laboratory temperature undergoes variations from ~10°C in the morning to ~20°C in the afternoon. The carbon monoxide (CO) monitor was installed by the Swiss Federal Institute for Materials Science and Technology (Empa)/MeteoSwiss in August of 2002. MKN joined the National Oceanic and Atmospheric Administration (NOAA) flask sampling program in December of 2003. The precipitation sampling program has not been initiated yet because of difficulties in the organization of sample analysis. Analytical equipment for rain samples is not currently available in Kenya, and samples would need to be sent routinely to other laboratories. These arrangements proved to be more difficult than expected, and a final solution is still pending. Additional information on the MKN site can be found on the GAW Station Information System Web site (http://www.empa.ch/gaw/gawsis/). Complementing the in situ measurements at Mount Kenya and strongly supported by MeteoSwiss, the ozone (O_3) sounding program in Nairobi, about 100 km south of the mountain, has been a very successful part of the Southern Hemisphere Additional Ozonesondes (SHADOZ) network (Thompson et al. 2004).

TABLE 1. Instrumentation of the Mount Kenya GAW site.

Parameter	Principle	Manufacturer/model	Period of operation	Sampling interval
Temperature	PT100	Vaisala HMP35D	1999–present	Continuous
Pressure	Aneroid barometer	Vaisala DPA21	1999–present	Continuous
Humidity	Humicap	Vaisala HMP35D	1999–present	Continuous
Wind speed	Cup anemometer	Vaisala WAA-15A	1999–present	Continuous
Wind direction	Wind vane	Vaisala WAV-15A	1999–present	Continuous
Solar radiation (direct, diffusive)	Thermopile-based pyranometer	Two Kipp and Zonen CM11 (one with manually adjustable shadowband), Kipp and Zonen CM121	1999–present	Continuous
Surface ozone	UV absorption	Thermo Electron Corporation TEI 49	1999–present	Continuous
Carbon monoxide	IR absorption	Thermo Electron Corporation TEI 48C TL	2002–present	Continuous
Black carbon	Filter and light attenuation (aethalometer)	Magee Scientific AE16 AE21	2002–03 2005–present	Continuous
Other trace gases	Flask sampling	NOAA/Global Monitoring Division	2004–present	Weekly
Precipitation	Precipitation sampler		Not yet in operation	
Column ozone (Nairobi)	Electrochemical concentration cell sounding	EnSci 2Z (Thompson et al. 2003)	1998–present	Weekly
	Microtops II spectrometer	Dobson No. 18	2005–present	Daily

b. Data

All 1-min data used in this analysis were checked for plausibility and were visually inspected. Obviously erroneous data were flagged as invalid. Weekly station log files maintained by the station operators were evaluated and served as another valuable source of information in the quality control process. From the 1-min data, longer time aggregates were compiled. Aggregates were only accepted when the coverage exceeded 45% and are reported in UTC [local standard time (LST) = UTC + 3; the time stamp reflects the end of the period].

The data presented here span the period from June of 2002 to the end of June of 2006. For this period, 1-h aggregates of the meteorological parameters were available for about 55% of the time; this number decreased to 50% for measurements of O_3 and CO (not discussed in this publication; see Henne et al. 2008). Longer periods of power failure were experienced in September of 2003, from October of 2004 to February of 2005, and in August of 2005, when the conditions of the access road did not permit mending of the power line. All MKN data used in this study as well as measurements of O_3 and CO are available through the GAW World Data Center for Greenhouse Gases (http://gaw.kishou.go.jp/wdcgg/).

Sunshine duration was not measured directly, but was derived by comparing measured global radiation with calculated global radiation. A simple parameterization of the atmosphere's transmissivity under cloud-free conditions (Stull 1988) and the solar zenith angle derived from the time of the year (Madronich and Flocke 1999) were used to calculate potential solar radiation. Sunshine conditions were then defined as times when the measured and calculated solar radiation deviated by less than 50 W m^{-2}. Furthermore, calculated radiation had to be larger than 100 W m^{-2} to avoid uncertainties of the calculation and the measurement around dusk and dawn. This analysis was performed on 1-min data. Hourly sums of sunshine duration were then aggregated and used for further analysis.

Cloud-free hours were defined as hours with more than 55 min of sunshine per hour. Because of the uncertainty in the estimation of sunshine duration, the threshold of 55 min was used rather than 60 min. Therefore, we might slightly overestimate the occurrence of cloud-free periods. No estimation of cloudiness was possible during nighttime. Cloud-free days were defined as days with at least 11 cloud-free hours. Because of a lack of visibility measurements, times at which the station was within clouds were defined as times when relative humidity exceeded 99%. Because large relative humidity might not only occur within clouds but also during or after rain events, our estimate of times within clouds is an upper limit.

In addition to the measurements at Mount Kenya, we analyzed radio soundings of temperature, humidity, and wind, operationally performed in Nairobi by the Kenyan Meteorological Department. These covered the period 2001–06 and were usually taken at 0000 UTC. Only in 2001 and 2002, additional soundings were carried out at 1100 or 1200 UTC. A simple parcel method was used to derive convective boundary layer (CBL) height from the noon soundings using a surface excess temperature of 0.5°C (Seibert et al. 2000). A second estimate of the CBL height was derived daily for 2001–06 from European Centre for Medium-Range Weather Forecasts (ECMWF) operational analyses (T511L60 extracted to 1° horizontal resolution) by applying the method described by Stohl et al. (2005).

4. Results

a. Diurnal cycle

Being situated at the slope of Mount Kenya, the GAW station is influenced by the development of thermally induced wind systems. The near vicinity to the equator favors strong solar radiation during the whole year. The mean diurnal cycle of solar radiation at the station (Fig. 4a) indicated clear-sky conditions for most of the morning hours until 1000 LST (0700 UTC). The diurnal cycle of sunshine duration (Fig. 4b) indicated that, later in the day, the station was often obscured by convective clouds forming over the crest of the Mount Kenya massif. During the last hour before sunset, clouds started to dissolve again and sunshine duration increased again. This pattern of cloud formation was very stable throughout the whole observation period (Fig. 5a). On more than 80% of all days the first hour after sunrise was cloud free, whereas this number decreased to less than 5% in the afternoon hours. Just before sunset the clouds vanished on 60% of all days. Because of its high elevation, the Mount Kenya GAW station often lay within clouds. Inverse to the diurnal cycle of cloud-free conditions, within-cloud conditions (Fig. 6a) most frequently occurred during the afternoon hours, when the station was within clouds on about 20% of all days. During nighttime and in the early morning hours the station was within the clouds less than 5% of the time.

As a consequence of the strong solar radiation in the morning hours, temperatures (Fig. 4c) within the slope layer increased sharply after sunrise until the time when cloud formation set in. Thereafter temperatures decreased slowly until sunset, followed by a sharp de-

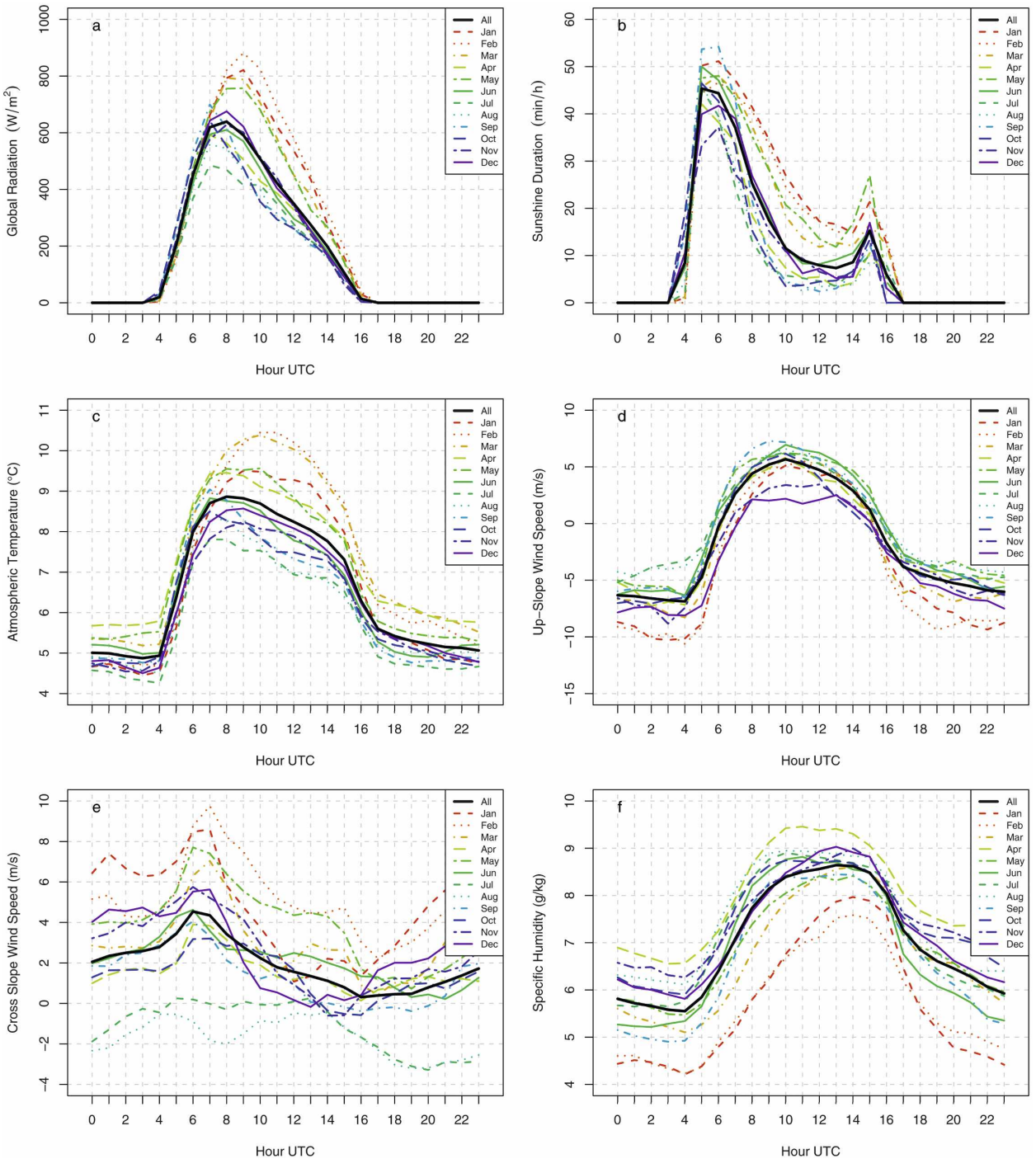

FIG. 4. Average diurnal cycle (black lines) for (a) global radiation, (b) sunshine duration, (c) ambient temperature, (d) upslope wind speed, (e) cross-slope wind speed (positive values refer to northeasterly wind; negative values indicate southwesterly wind), and (f) specific humidity. The colored lines correspond to diurnal cycles of individual months (see legend).

crease after sunset. Nighttime temperatures remained constant with a moderate decrease during the course of the night. Slope wind circulations (Fig. 4d) emerged, counteracting the temperature differences between slope wind layer and the less heated or cooled free troposphere, resulting in daytime upslope and nighttime downslope wind. Note that the temperature was slowly decreasing in the afternoon hours whereas it was

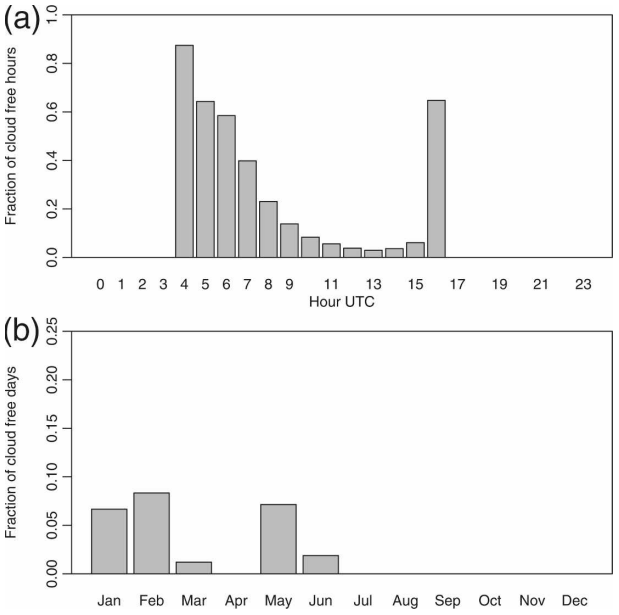

FIG. 5. (a) Diurnal cycle of fraction of cloud-free hours, and (b) annual cycle of the fraction of cloud-free days.

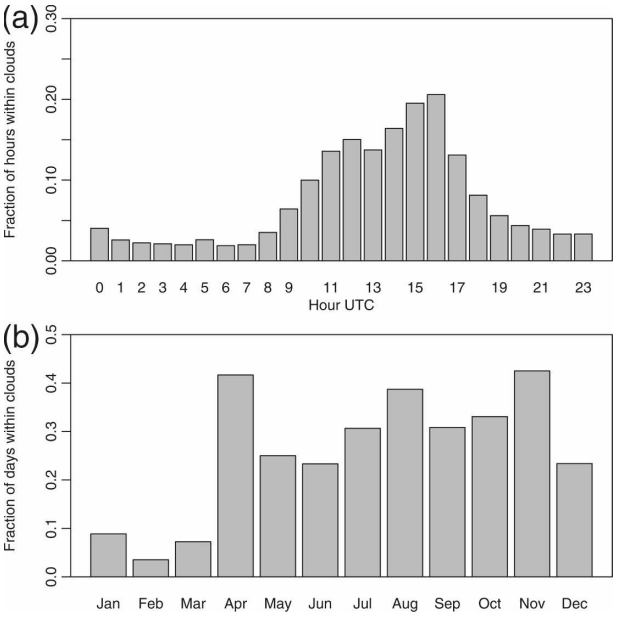

FIG. 6. (a) Diurnal cycle of fraction of hours within clouds, and (b) annual cycle of days with at least 1 h within clouds.

sharply increasing in the morning hours although solar radiation was similar for both periods. These observations are explained as follows: First, the depth of the slope wind layer is small for nighttime katabatic flow relative to daytime anabatic flow; therefore sensible heat is dispersed in a much smaller volume of air in the early morning and can cause larger heating of this layer relative to afternoon hours. Second, the temperature advection of the slope wind flow has to be considered. During the period of strongest temperature increase (0400–0600 UTC) the slope winds are still directed downward and therefore, within a stably stratified atmosphere, present an additional adiabatic warming. Once the upslope flow is established the temperature increase slows down because of the additional adiabatic cooling of ascending air and the temperature even starts to decrease again when solar radiation decreases as a result of cloud formation. The absolute wind speed of the cross-slope wind (Fig. 4e; perpendicular to the upslope direction, with positive values indicating northeasterly winds) showed a maximum when the absolute upslope/downslope wind ceased in the morning hours during the transition from down- and upslope flow. At this time of the day the temperature differences between the slope layer and the free atmosphere were small and the synoptically driven wind could penetrate down to the surface. Larger specific humidity (Fig. 4f) was observed during daytime than during nighttime, indicating transport of moist air from lower altitudes with the upslope wind, and transport of dryer air with the downslope wind. The diurnal cycles of slope wind and specific humidity were almost in phase, indicating that the transported humidity did not remain within a finite volume of air around the site but was rather horizontally transported away from the mountain area. Otherwise a 90° phase shift between the diurnal cycle of wind speed and humidity could have been expected. Because the station is surrounded by a swamp area, additional water vapor from evapotranspiration has to be expected during the day in the slope wind layer. This increased local humidity might alter nighttime radiative cooling to be less effective than under dry conditions.

The local wind velocities at MKN (Fig. 7a) showed a strong bidirectional distribution with up- and downslope wind directions dominating the distribution. The distribution was slightly asymmetric with more frequent occurrences of downslope motion. The division in up- and downslope direction was even more apparent when the data were split into daytime and nighttime data (Figs. 7b,c). During the day, upslope winds (northwest–north-northwest) dominated at the station. Most of the daytime wind speeds larger than 10 m s^{-1} had a cross-slope component from north and north-northeast. Nighttime winds were essentially in the downslope direction (southeast). Wind speeds larger than 10 m s^{-1} were more frequent in the sectors east to south-southeast than in the southern sector. During the transitional period, all wind directions were prominent, with stronger wind speeds from the east. At the same time, downslope winds were about 3 times as frequent

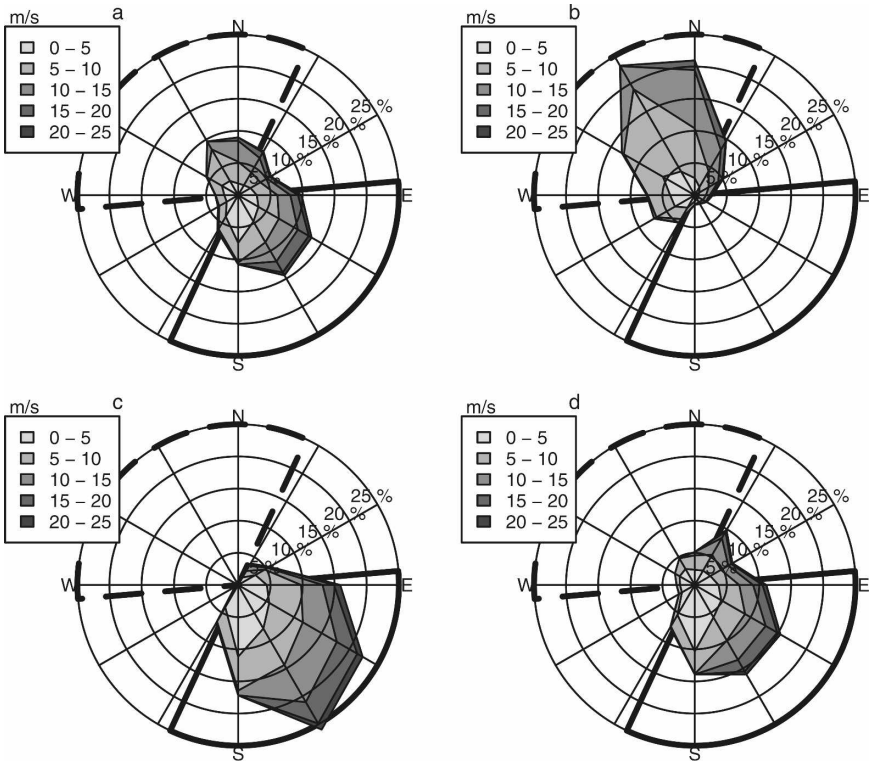

FIG. 7. Wind distribution at Mount Kenya GAW station: (a) all data, (b) daytime (0800–1500 UTC), (c) nighttime (2000–0300 UTC), and (d) transitional, or remaining, hours (1600–1900 and 0400–0700 UTC). The upslope wind sector is surrounded by the thick dashed line, and the downslope wind sector is indicated by the thick solid line. The percentages give the cumulative probability for each of the 12 analyzed wind sectors.

as upslope winds (Fig. 7d; each of the three wind sectors within the upslope wind sector accounts for about 5% of all wind measurements during the transition phase, whereas the three wind sectors within the downslope wind sector account for about 15% each).

b. Annual cycle

Throughout the year, Kenya is influenced by two distinctly different wind regimes (northeasterly winds in boreal winter; southeasterly winds during boreal summer) and two rainy seasons when the ITCZ crosses the equator. Therefore, seasonal variations in the diurnal weather patterns developing at Mount Kenya can be expected. Afternoon global radiation (Fig. 4a) was above average from January to March and in May and was below average during April and from July to October. The same pattern was observed for sunshine duration (Fig. 4b). Entirely cloud free days (Fig. 5b) were very rare, with a maximum of about 10% of all days during January–February and in May. Within-cloud conditions (Fig. 6b) were observed on 20%–40% of all days of a month during most of the year but were below 10% for the months of January–March.

This annual pattern observed for the northwestern side of Mount Kenya contrasts with the expectation of increased cloudiness during the rainy seasons. Decreased sunshine duration was indeed observed during April (Fig. 4b), the core month of the long-rains period, but the short-rains period (October–November) was preceded by a period of decreased sunshine duration from July to October. Cloud formation at Mount Kenya is mainly driven by the convergence of the upslope wind around the crest area of the mountain. The local wind system, however, interacted with the synoptic wind in a way that clouds were blown toward the lee of the mountain. Northeasterly synoptic winds in boreal winter therefore tended to reduce cloudiness over the station whereas southeasterly to southerly winds during boreal summer tended to increase cloudiness over the station.

The less frequent formation of afternoon clouds from January to March led to a displacement of the diurnal temperature maximum from around 0800 to 1000 UTC and to an increase in the temperature amplitude (Fig. 4c). In general, temperatures were about 1°C warmer from February to May than from July to December.

The more pronounced diurnal cycle of temperature also induced a stronger slope wind system, resulting in a larger amplitude of the upslope wind speed cycle during January and February. The larger amplitude was mainly due to stronger nighttime downslope winds. Furthermore, there was a distinct seasonal difference for the cross-slope wind speed (Fig. 4e), which exhibited generally stronger cross-slope wind speeds in January, February, and May.

Specific humidity (Fig. 4f) exhibited larger diurnal amplitude during January–February, even if the specific humidity in general was lower than in other months. This agrees with the arrival over Kenya of relatively dry air masses advected from India and Arabia over a relatively short section of the northern Indian Ocean. In contrast, during boreal summer air has been transported over longer distances over the southern Indian Ocean. April (long rains) showed the largest specific humidity whereas no systematic increase in specific humidity could be seen in November (short rains). The time of the diurnal maximum of specific humidity was shifted to later hours during November–March relative to May–October. In general, the diurnal patterns observed at MKN dominated over the seasonal patterns. The mountain creates its own mesoclimate.

c. *Categorization of air masses*

The daytime influence of the moister atmospheric boundary layer dominates the monthly-average diurnal cycle throughout the whole year. However, there might be days that fully represent undisturbed free tropospheric conditions. To select these, two independent filters for days with free tropospheric conditions based on the course of the local wind (the possible driver for the moisture increase) and specific humidity q (the indicator of moisture increase) were developed.

For the first criterion, days were categorized as thermally or synoptically influenced days, based on the assumption that thermally induced wind systems were the main driver for boundary layer influence. To this end, up/downwind sectors were defined as $\pm 60^\circ$ from the up/downslope direction (Fig. 7). Thermal influence was assigned when upslope winds occurred during at least two daytime hours and downslope winds occurred during at least two nighttime hours. In a second step, to detect days that showed constant wind direction for most of the day but arbitrary fluctuations in the up/downwind direction and would therefore be categorized as thermally driven days, the steadiness of the 1-h vector mean wind (Singer 1967) was evaluated for 24-h periods. Steadiness of wind uses the fraction of the scalar average of wind speed with respect to the vector average wind speed to characterize the variability of the wind direction during the averaging period. Steadiness of wind varies between 0 (completely symmetrical wind distribution) and 1 (constant wind direction). Wind measurements at sites that are not influenced by diurnally developing thermally induced wind systems show large steadiness (>0.8) on the 24-h aggregation level (Singer 1967). We chose a threshold steadiness of 0.63 (the median steadiness on days without thermally induced wind systems at MKN as according to the first step of the selection criterion). From a total of 548 days with complete data coverage for all necessary meteorological parameters, 78 were selected by the wind criterion as not showing a pronounced up-/downslope pattern. The additional steadiness threshold selected 12 additional days as not being thermally influenced so that in total 90 days were categorized as synoptically (labeled syn) and 458 days as thermally (labeled therm) influenced.

Using a second independent criterion, we identified days that showed a significantly (two-sample t test; $p < 0.05$) higher daytime (1300–1600 UTC) than nighttime (0100–0400 UTC) specific humidity. A similar approach to identify boundary layer influenced days at the high Alpine site Jungfraujoch, Switzerland, was applied by Zellweger et al. (2003) for specific humidity and total oxidized nitrogen (NO_y) mixing ratios and could be applied for any additional atmospheric composition parameter. This second criterion categorized 415 days as days with variable specific humidity (labeled var) and 133 as days with "constant" specific humidity (labeled const).

The two criteria should be seen independently. However, frequent co-occurrence of thermally driven wind systems and increased specific humidity would identify this mechanism as the main driver of boundary layer air transport. Combining both criteria, the largest fraction of all days (365 days, 67%) was categorized as thermally influenced with variable q (therm/var) and 93 days (17%) were attributed as thermally influenced with constant q (therm/const). Of the synoptically influenced days, 50 days (9%) showed a significant increase in daytime q (syn/var), whereas 40 days (7%) showed no increase (syn/const). Therefore, the main reason for elevated moisture levels in the afternoon hours can be seen in thermally induced wind systems. On 74% of all days the moisture development can be explained by the presence or absence of slope wind circulations.

The diurnal cycles for the combined categories differed distinctly (Fig. 8). In general, a more pronounced division was observed between the synoptically and thermally influenced regimes than between constant and variable q. Synoptically influenced days were characterized by higher solar radiation, temperatures, and

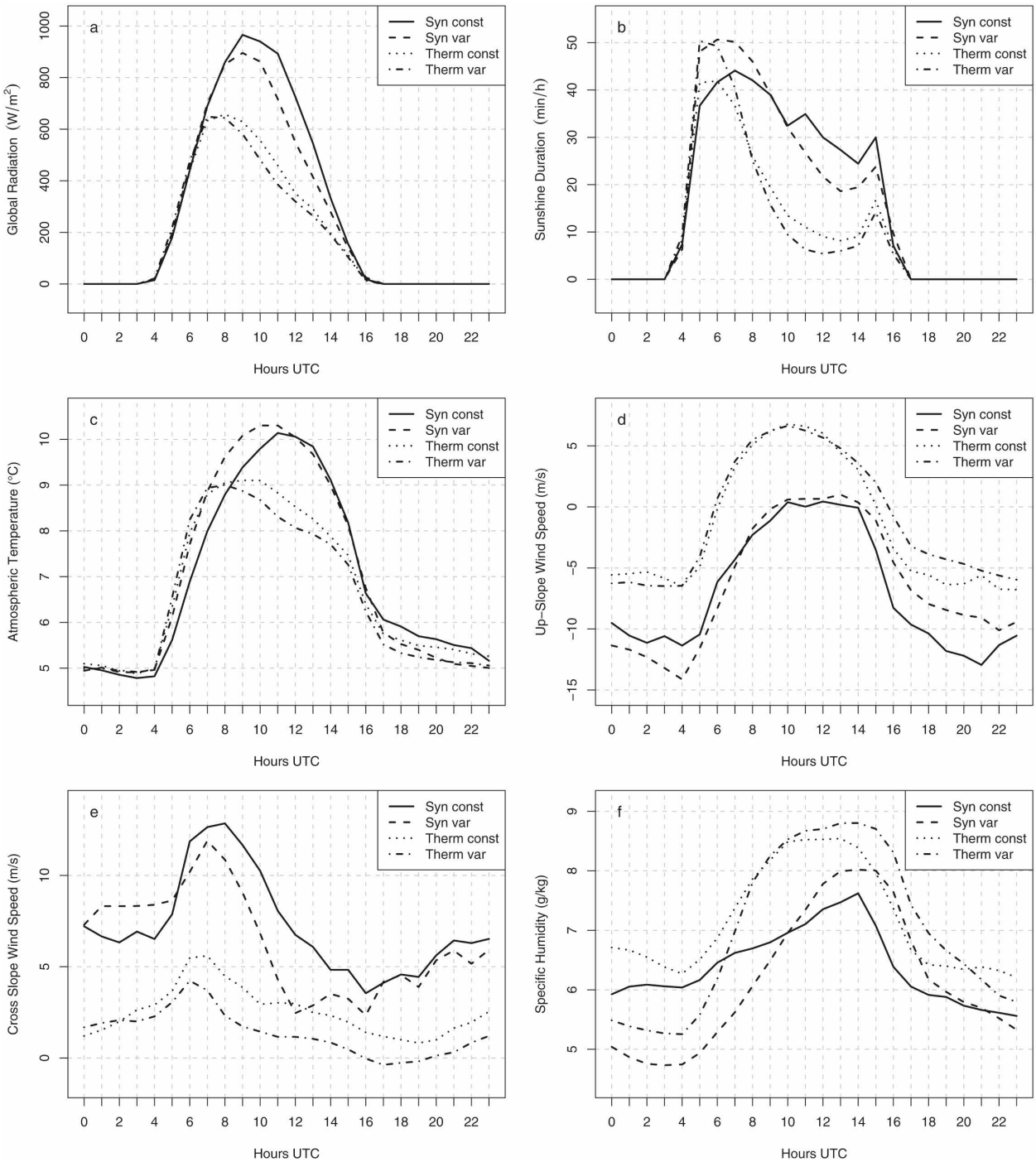

FIG. 8. Diurnal cycle for (a) global radiation, (b) sunshine duration, (c) ambient temperature, (d) upslope wind speed, (e) cross-slope wind speed, and (f) specific humidity, for different selection criteria (see text for details).

wind speeds (Fig. 8). It is likely that large wind speeds reduced convective cloud formation over the mountain, and strong solar radiation was also received in the afternoon hours leading to increased temperatures. Thermally induced wind systems also developed on synoptically influenced days (Fig. 8d); however, downslope wind during nighttime was stronger and only weak (<1 m s^{-1}) or no upslope wind developed during daytime.

On average, all categories showed a daytime increase in specific humidity (Fig. 8f). Nevertheless, distinct dif-

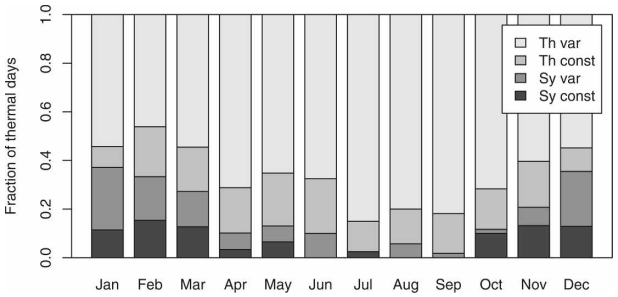

FIG. 9. Fraction of days per selection criteria by month.

ferences resulted for the different individual categories. The most pronounced daytime increase was observed for the therm/var category, for which specific humidity increased sharply after sunrise, leveled off around 0900 UTC, and peaked in the late afternoon around 1400 UTC. A similar daytime pattern was observed for the therm/const category. However, q was more elevated during nighttime. The syn/const category also exhibited large nighttime specific humidity, but the daytime increase was slower in comparison with the thermally influenced days and peaked at lower absolute values. The category syn/var peaked at the same time in the afternoon but showed the lowest nighttime q. Synoptically influenced days exhibited narrower daytime peaks of q that occurred somewhat later in the afternoon.

Thermally influenced days showed a broad daytime maximum in q that revealed signs of a double peak structure. They also occurred more frequently during boreal summer, when ~90% of all days were categorized as thermally influenced (Fig. 9). During boreal winter this fraction decreased to 60%–70%. This seasonal difference mainly resulted from variations in the category therm/var. Within the synoptic categories, cases with variable q were more frequent than cases with constant q for all months except October–November. Days with constant q, whether on thermally or on synoptically influenced days, were most frequent (about 30%) in February, March, and November.

d. Turbulent vertical mixing

Besides direct vertical transport in thermally induced wind systems, vertical mixing of boundary layer air might influence the measurements at MKN. We investigated the depth of the daytime CBL (Fig. 10) to distinguish its influence on MKN.

CBL heights were analyzed at 1200 UTC (1500 LST),

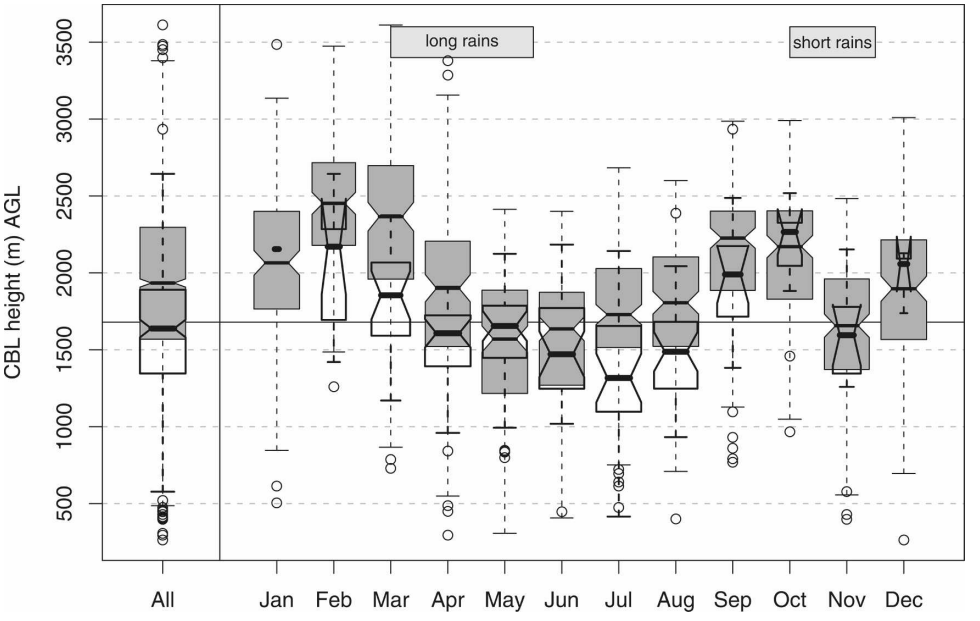

FIG. 10. Distribution and annual cycle of maximum CBL height above ground as determined by Nairobi radio soundings (open boxes; 262 noon soundings during 2001–06) and as taken from ECMWF analysis (shaded boxes; daily for 2001–06). The horizontal line represents the Mount Kenya station altitude relative to the terrain northwest of the mountain. The central line of each box represents the median value, the upper and lower sides of the boxes represent the 75th and 25th percentiles, respectively, and the upper and lower whisker refer to the highest and lowest values, respectively, within 1.5 interquartile range. Values outside this range are marked by open circles. The notches give the 95% confidence interval for the median. The width of the individual boxes is proportional to the data availability in each month. The horizontal boxes at the top of the figure represent the rainy periods in Kenya.

close to the time of their expected daily maximum. The annual median CBL height, as determined from radio soundings in Nairobi, was 1640 m above ground level (AGL), whereas the annual median CBL height taken from ECMWF analysis and interpolated to the position of MKN was 250 m larger (Fig. 10). CBL heights retrieved with both methods showed a significant correlation ($r = 0.66$; $p < 0.01$) and large scatter ranging from less than 500 m AGL to as high as 3500 m AGL.

The annual cycle of CBL heights was similar for both estimation methods. In general the CBL was shallower during the boreal summer than during boreal winter, which is due to the fact that the trade wind inversion is rising toward the ITCZ and the ITCZ is farthest away from Kenya during boreal summer. The CBL depth was larger during the months preceding the rainy seasons (February–March and September–October), and it was smaller during the rainy seasons. Furthermore, mixing layer depth was reduced after the rain season relative to the mixing depth directly before the rain season. Two factors might be responsible for this reduction: first, the decreased solar radiation in comparison with the solar zenith in March and September, and, second, the moister surface conditions after the rain season. Both would lead to a reduction of the surface sensible heat flux, possibly lowering the mixing height.

If we assume that the CBL top does not follow the isolated Mount Kenya mountain topography, we can compare the calculated CBL height with the altitude of MKN (3680 m MSL) relative to the altitude of the surroundings to the northwest (1800–2000 m MSL). This comparison indicates that in about 50% and 75% of all cases, the maximum CBL (retrieved from the soundings and analysis, respectively) reached above the station (Fig. 10). During boreal winter, the maximum CBL top reached above the station on most days, whereas during boreal summer this was only the case for less than 50% of all days.

Because only a limited number of daytime radio soundings were available for CBL height estimation, inversion layers retrieved from daytime and nighttime soundings from Nairobi were used as a proxy for CBL depth. A strong inversion layer can often be seen as the upper limit of CBL development, although its height does not necessarily correspond to the CBL top. Only inversion layers with a temperature difference larger than 0.5°C and below 3700 m MSL were considered. Inversion layers were prominent throughout both dry seasons. On 60% and 80% of all days inversion layers could be observed during boreal winter and summer, respectively (Fig. 11). During the rainy seasons inversion layers were less prominent, 30%–40%, in agreement with the presence of the ITCZ over the region. As

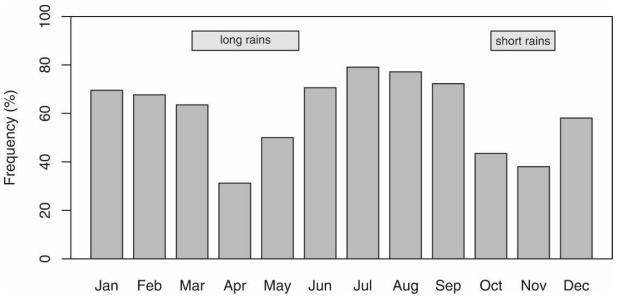

FIG. 11. Percentage of days with an inversion layer ($\Delta T > 0.5$ K) below 3700 m MSL, based on radio soundings from Nairobi for 2001–06.

shown in Figs. 10 and 11, minima in the occurrence of inversion layers were directly connected to the rainy seasons and were lagging 1–2 months behind maxima in CBL depths. The reduced CBL height during the rainy season can be explained by increased cloud cover, and fewer inversions (reduced atmospheric stability) are in line with more frequent deep convective activity during the rainy season.

5. Discussion

The diurnal variations in the meteorological variables at MKN reported in this manuscript support previous observations of diurnal variations of CO_2 and CN at different sites on the mountain and during individual aircraft soundings up to 5500 m MSL (Schnell 1978a). They are also in agreement with previous meteorological observations made in the Mount Kenya peak region in 1975 (Davies et al. 1977, 1979) that indicated a generally stable atmosphere in which two distinct haze layers exist and where downslope wind dominates at dawn. The haze layers dispersed during the day because of insolation and upslope wind. Upslope wind and the rising of the haze layer carried near-surface pollution up toward the peak area.

We were able to distinguish the same two processes: thermally induced wind systems and rising convective boundary layer top (haze layer). Our criterion based on wind measurements successfully selected days that showed little or no development of thermally induced wind systems. However, the average afternoon peak in specific humidity remained evident in all categories, even on days that were synoptically influenced and where the increase in specific humidity was not significant. Part of the additional afternoon moisture might be attributed to local evapotranspiration. A similar afternoon increase was also observed for all meteorological categories for carbon monoxide mole fractions (Henne et al. 2008). Because there are no local carbon

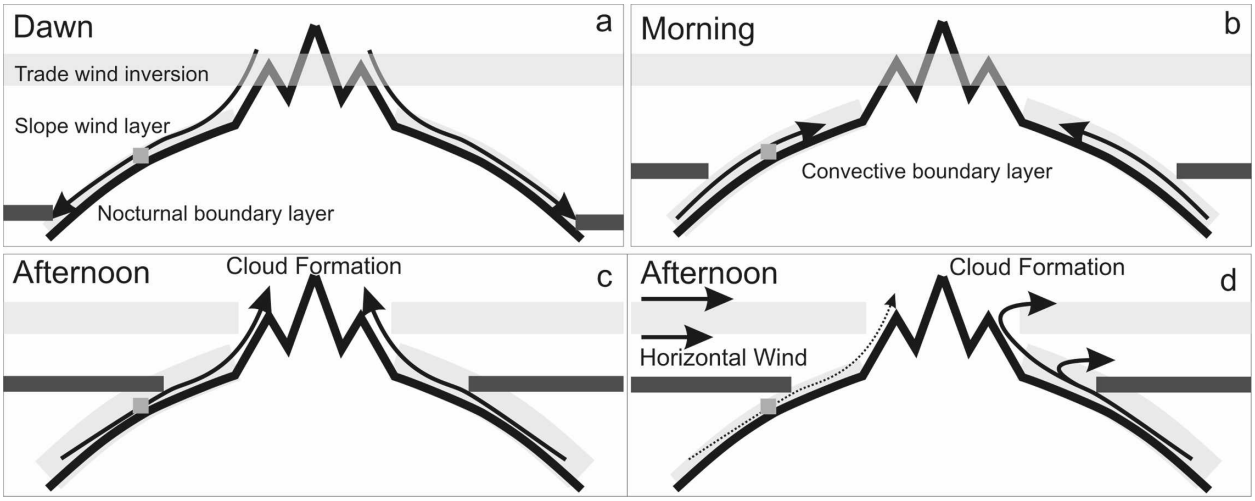

FIG. 12. Schematic of slope flow and vertical atmospheric structure at Mount Kenya [extending an earlier sketch by Davies et al. (1979)]: (a)–(c) diurnal development of the vertical structure under weak horizontal flow conditions and (d) afternoon flow structure under strong horizontal flow conditions. The square at the left slope of the mountain indicates the approximate position of the Mount Kenya GAW station.

monoxide sources on the mountain itself, this result supports the conclusion of influence by the more polluted atmospheric boundary layer and argues against the importance of local evapotranspiration at the site.

Convective mixing transports moisture and pollutants up to the station during daytime. Maximum CBL depth can be expected in the late afternoon. This coincides with the time of the moisture maximum that was observed on days without formation of thermally induced wind systems. Therefore, we conclude that turbulent mixing was responsible for the afternoon increase. On days with thermally induced wind systems there is an indication of a double peak in specific humidity, where the time of the second maximum coincides with the maximum observed on days without thermally induced wind systems. Hence, it can be assumed that on days with thermally induced wind systems both processes, direct upward transport in the slope wind system and turbulent mixing in the mountain environment, act together and efficiently transport moisture and boundary layer pollutants toward the station. In contrast, the station experiences air of free-tropospheric origin during nighttime katabatic flow conditions. The typical diurnal development of the atmospheric structure and thermally induced flow systems around Mount Kenya on days with weak large-scale horizontal advection is shown in Figs. 12a–c. The height of the trade wind inversion will typically be lower than the top of the mountain. During nighttime, air is transported downhill in a shallow nocturnal slope wind layer. The altitude of the nocturnal boundary layer of the surroundings is far below the altitude of the GAW site. In the morning this boundary layer becomes convective and its top starts to rise but is still below the MKN station. Upslope flow develops and directly carries moister air toward the site and farther up the mountain. After local noon the convergence of the upslope flows over the crest area is strong enough to initialize cloud formation, locally breaking up the trade wind inversion. The convective boundary layer of the surroundings reaches its maximal vertical extent, which might be higher than the site, in which case air sampled at the site originates from the top of the convective boundary layer.

Although thermally induced circulations and convective mixing are fed by the same source of energy (sensible heat flux at the surface) their strength and extent also depend on atmospheric stability. On one hand, during periods with increased atmospheric stability or when strong inversions are present at lower levels, the top of the convective boundary layer will be suppressed and—in the case of Mount Kenya—might be well below the observatory, and slope flows will only weaken under such conditions but still enable some vertical transport (Vergeiner and Dreiseitl 1987). On the other hand, in near-neutral conditions convective mixing in the slope wind layer might become so strong that only a weak temperature gradient toward the free troposphere develops and slope flows will actually decrease (Henne et al. 2005: Vergeiner and Dreiseitl 1987). As a consequence, CBL heights were larger from December to March when thermally induced wind systems were least frequent, so that boundary layer air could still influence the station. Further, the development of ther-

mally induced wind systems was most frequent during boreal summer when atmospheric stability was strongest and CBL heights were lowest. Therefore, daytime transport of boundary layer pollutants toward the station can be expected for most days of the year.

The combined criterion based on wind and specific humidity is not able to select days with completely undisturbed free tropospheric conditions. Background conditions with respect to atmospheric composition can only be expected at nighttime. Because specific humidity decreased fastest during 1500–1800 UTC, slowly decreasing further throughout the whole night and exhibiting a minimum at 0400 UTC, we assert that nighttime data from 2100 to 0400 UTC are most likely to represent background conditions. However, the increased nighttime specific humidity during days on which the daytime increase was not significant points to the presence of residual atmospheric boundary layer air masses during nighttime. Therefore, even days without a significant increase in specific humidity may not always represent free-tropospheric conditions. This notion is also supported by the observation that the months with the deepest mixing layer coincide with the months showing the most frequent occurrence of increased nighttime specific humidity. Under such conditions it might be necessary to further restrict the free-tropospheric sampling interval to 0000–0400 UTC or to discard such days completely.

Filters similar to the one described here were used for other high-altitude observatories such as Mauna Loa (Atlas and Ridley 1996) and Jungfraujoch (Nyeki et al. 1998). For Mauna Loa, Whittlestone et al. (1996) demonstrated the use of ^{212}Pb (lead isotope) measurements to further exclude cases in which air masses sampled during nighttime were in recent contact with the earth's surface. For Jungfraujoch, where in contrast to Mount Kenya, transport mechanisms other than thermally induced wind systems and turbulent mixing can play an important role, further meteorological filters for föhn conditions, frontal lifting, and wet convective mixing have been developed (Forrer et al. 2000). Furthermore, cases of thermally induced wind have been detected by using regional-scale meteorological information (Henne et al. 2005) or by directly using atmospheric composition measurements (Zellweger et al. 2003).

To understand the seasonal pattern of the thermally induced circulation at MKN, one must consider the location of the station relative to the mountain crest and the seasonally varying horizontal winds. The East African climate was described in detail by Asnani (1993) and a seasonal transport "climatology" for the period 1991–93 was presented by Gatebe et al. (1999). Furthermore, airflow regimes for the period investigated here are discussed by Henne et al. (2008). The strongest winds close to the surface over central Kenya are experienced during boreal winter when advection below 5000 m MSL is from the northeast (Fig. 13). Under these conditions the station is on the windward side of the mountain and the strong horizontal winds can efficiently destroy the temperature gradient between the slope wind layer and the free atmosphere and therefore suppress organized slope winds, whereas these can still develop on the leeward side of the mountain (Fig. 12d). Although, as described before, the EALLJ at the Kenyan coast is strongest during boreal summer, wind speeds over central Kenya are smaller and advection close to the surface is from the southeast while it turns to northeasterly directions above 4000 m MSL (Fig. 13). In addition to the weaker winds, MKN is situated on the leeward side of the mountain during boreal summer. This interaction between larger-scale horizontal winds and thermally induced circulations directly explains the observed minimum (maximum) of thermally influenced days in boreal winter (summer). This seasonal pattern agrees with observations of the slope wind frequency at the Mauna Loa Observatory (19.54°N, 155.58°W, 3400 m MSL) that is located at the slope of a similarly shaped mountain and is under similar alternating influence of the trade wind direction (Mendonca 1969).

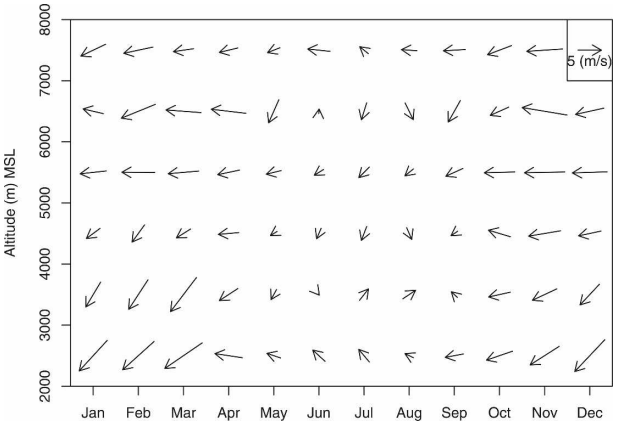

FIG. 13. Vertical profile of annual cycle of vector mean horizontal wind speed and direction estimated from radio soundings from Nairobi for 2001–06. Note that the altitude of the sounding site is 1800 m MSL.

The meteorological variability at MKN is determined by the diurnal and, to a lesser extent, by the annual cycle of varying advection patterns. Interannual variability of the East African climate is small relative to the seasonal cycle. Anomalies in rainfall in East Africa, especially during the short rains period, have been re-

lated to sea surface temperature anomalies in the Indian Ocean and the Indian Ocean dipole that lead to the reversal of the zonal circulation (Slingo et al. 2005). The influence of the 40–50-day oscillation (Madden and Julian 1994), which originates in the western Indian Ocean, on the weather of equatorial East Africa is limited because the disturbance travels eastward. Tropical cyclones form in the eastern Indian Ocean and travel westward; however, they are deflected southward or northward from the equator, and their influence on equatorial East Africa remains small (Slingo et al. 2005). Therefore, we expect our findings for the period 2002–06 to hold for other years as well.

6. Conclusions

The meteorological observations at the Mount Kenya GAW station prove the successful installation and commissioning of a GAW station in a remote tropical environment under difficult logistic conditions. The site is frequently influenced by cloud formation, and during the afternoon hours the site was within clouds on about 20% of all analyzed days. Thermally induced slope winds dominate the local transport of air toward the station (86% of all days), transporting more polluted atmospheric boundary layer air toward the site during daytime. Applying selection criteria based on wind and humidity, it was possible to separate thermally influenced days from synoptically influenced days. However, even for the latter, atmospheric boundary layer influence was identified during the afternoon and was attributed to mixing in the convective boundary layer reaching the altitude of the site.

In general, the station conforms to the siting criteria for GAW sites. However, the transport of boundary layer air masses during daytime requires selection of nighttime measurements for any long-term trend analysis of background atmospheric composition. Daytime samples reflect a mixture of free tropospheric and boundary layer air and are therefore not representative of larger-scale conditions, although they are still very useful for the characterization and trend analysis of the rural atmospheric boundary layer over Kenya. Trends in the atmospheric boundary layer might differ significantly from the free tropospheric trend because of regional emission increases, as shown for example for southern Africa by Diab et al. (2004). Anticipated population growth and continued industrialization within Kenya will increase trace gas emissions in the near future.

When focusing on atmospheric background conditions, use of daytime measurements from the Mount Kenya GAW station is not recommended because they almost always show signatures of boundary layer influence. However, one-third of all measurements at MKN (obtained between 2100 and 0400 UTC) generally represent free-tropospheric conditions. Further data filtering might be necessary to identify local pollution events (e.g., biomass burning within the local forest) and to identify residual layer influence. To derive background time series, extreme events should be identified by the application of statistical methods to the in situ measurements or by application of Lagrangian particle dispersion models to identify the station's catchment area. Because MKN is situated at the equator, it is influenced by distinctly different air masses throughout the year. Trace gas trends might considerably differ within these air masses because of variable emission trends in the different source regions. In a companion publication, the influence of air mass origin on the Mount Kenya trace gas measurements based on backward trajectories is analyzed in detail (Henne et al. 2008). A substantial part of interhemispheric exchange during boreal summer takes place within the East African low-level jet (Findlater 1969b). Although the site is situated at the western edge of this flow, it is well suited for the study of hemispheric pollutant budgets.

Acknowledgments. The installation of the Mount Kenya GAW station was financed by WMO and the World Bank. This work was financially supported by MeteoSwiss. We acknowledge the support of the Mount Kenya National Park authorities who grant access to the protected mountain site. We commend KMD for its commitment to the GAW program. We thank the anonymous referees for their valuable comments and suggestions. Last but not least, we express our gratitude toward the Mount Kenya GAW station operators who often have to work under harsh conditions.

REFERENCES

Asnani, G. C., 1993: *Tropical Meteorology*. Vol. 1. Noble, 603 pp.

Atlas, E. L., and B. A. Ridley, 1996: The Mauna Loa observatory photochemistry experiment: Introduction. *J. Geophys. Res.,* **101,** 14 531–14 541.

Brenninkmeijer, C. A. M., 1996: Global Atmosphere Watch adds six new stations. *Eos, Trans. Amer. Geophys. Union,* **77,** 109.

Davies, T. D., P. Brimblecombe, and C. E. Vincent, 1977: The daily cycle of weather on Mount Kenya. *Weather,* **32,** 406–417.

——, C. E. Vincent, and P. Brimblecombe, 1979: Condensation nuclei and weather on Mount Kenya. *J. Appl. Meteor.,* **18,** 1239–1243.

Diab, R. D., A. M. Thompson, K. Mari, L. Ramsay, and G. J. R. Coetzee, 2004: Tropospheric ozone climatology over Irene, South Africa, from 1990 to 1994 and 1998 to 2002. *J. Geophys. Res.,* **109,** D20301, doi:10.1029/2004JD004793.

Findlater, J., 1969a: A major low-level air current near Indian Ocean during northern summer. *Quart. J. Roy. Meteor. Soc.,* **95,** 362–380.

——, 1969b: Interhemispheric transport of air in lower troposphere over western Indian Ocean. *Quart. J. Roy. Meteor. Soc.,* **95,** 400–403.

Forrer, J., R. Ruttimann, D. Schneiter, A. Fischer, B. Buchmann, and P. Hofer, 2000: Variability of trace gases at the high-Alpine site Jungfraujoch caused by meteorological transport processes. *J. Geophys. Res.,* **105,** 12 241–12 251.

Gatebe, C. K., P. D. Tyson, H. Annegarn, S. Piketh, and G. Helas, 1999: A seasonal air transport climatology for Kenya. *J. Geophys. Res.,* **104,** 14 237–14 244.

Henne, S., M. Furger, and A. S. H. Prévôt, 2005: Climatology of mountain venting–induced moisture layers in the lee of the Alps. *J. Appl. Meteor.,* **44,** 620–633.

——, J. Klausen, W. Junkermann, J. M. Kariuki, J. O. Aseyo, and B. Buchmann, 2008: Representativeness and climatology of carbon monoxide and ozone at the global GAW station Mt. Kenya in equatorial Africa. *Atmos. Chem. Phys.,* **8,** 3119–3139.

Hulme, M., R. Doherty, T. Ngara, M. New, and D. Lister, 2001: African climate change: 1900–2100. *Climate Res.,* **17,** 145–168.

Leroux, M., 2001: *The Meteorology and Climate of Tropical Africa*. Springer, 548 pp.

Ma, J. Z., J. Tang, X. J. Zhou, and X. S. Zhang, 2002: Estimates of the chemical budget for ozone at Waliguan Observatory. *J. Atmos. Chem.,* **41,** 21–48.

Madden, R. A., and P. R. Julian, 1994: Observations of the 40–50-day tropical oscillation—A review. *Mon. Wea. Rev.,* **122,** 814–837.

Madronich, S., and S. Flocke, 1999: The role of solar radiation in atmospheric chemistry. *The Handbook of Environmental Chemistry: Part L Environmental Photochemistry,* Vol. 2, P. Boule, Ed., Springer, 1–26.

Mendonca, B. G., 1969: Local wind circulation on the slopes of Mauna Loa. *J. Appl. Meteor.,* **8,** 533–541.

Nyeki, S., F. Li, E. Weingartner, N. Streit, I. Colbeck, H. W. Gaggeler, and U. Baltensperger, 1998: The background aerosol size distribution in the free troposphere: An analysis of the annual cycle at a high-alpine site. *J. Geophys. Res.,* **103,** 31 749–31 761.

Schnell, R. C., 1978a: Some size and composition characteristics of aerosols at Mount Kenya, East Africa. *Bull. Amer. Meteor. Soc.,* **59,** 1519.

——, 1978b: Report on the Mount Kenya Baseline Station Feasibility Study. Rep., World Meteorological Organization, 171 pp.

Seibert, P., F. Beyrich, S. E. Gryning, S. Joffre, A. Rasmussen, and P. Tercier, 2000: Review and intercomparison of operational methods for the determination of the mixing height. *Atmos. Environ.,* **34,** 1001–1027.

Singer, I. A., 1967: Steadiness of the wind. *J. Appl. Meteor.,* **6,** 1033–1038.

Slingo, J., H. Spencer, B. Hoskins, P. Berrisford, and E. Black, 2005: The meteorology of the western Indian Ocean, and the influence of the East African highlands. *Philos. Trans. Roy. Soc. London,* **A363,** 25–42.

Stohl, A., C. Forster, A. Frank, P. Seibert, and G. Wotawa, 2005: Technical note: The Lagrangian particle dispersion model FLEXPART version 6.2. *Atmos. Chem. Phys.,* **5,** 2461–2474.

Stull, R. B., 1988: *An Introduction to Boundary Layer Meteorology*. Kluwer Academic, 666 pp.

Thompson, A. M., and Coauthors, 2003: Southern Hemisphere Additional Ozonesondes (SHADOZ) 1998–2000 tropical ozone climatology 1. Comparison with Total Ozone Mapping Spectrometer (TOMS) and ground-based measurements. *J. Geophys. Res.,* **108,** 8238, doi:10.1029/2001JD000967.

——, J. C. Witte, S. J. Oltmans, and F. J. Schmidlin, 2004: SHADOZ—A tropical ozonesonde–radiosonde network for the atmospheric community. *Bull. Amer. Meteor. Soc.,* **85,** 1549–1564.

Vergeiner, I., and E. Dreiseitl, 1987: Valley winds and slope winds—Observations and elementary thoughts. *Meteor. Atmos. Phys.,* **36,** 264–286.

Wang, T., H. L. A. Wong, J. Tang, A. Ding, W. S. Wu, and X. C. Zhang, 2006: On the origin of surface ozone and reactive nitrogen observed at a remote mountain site in the northeastern Qinghai-Tibetan Plateau, western China. *J. Geophys. Res.,* **111,** D08303, doi:10.1029/2005JD006527.

Whiteman, C. D., 1990: Observation of thermally developed wind systems in mountainous terrain. *Atmospheric Processes over Complex Terrain,* W. Blumen, Ed., Amer. Meteor. Soc., 5–42.

Whittlestone, S., S. D. Schery, and Y. Li, 1996: Pb-212 as a tracer for local influence on air samples at Mauna Loa Observatory, Hawaii. *J. Geophys. Res.,* **101,** 14 777–14 785.

World Meteorological Organization, 2001: Global Atmosphere Watch measurements guide. GAW Rep. 143/WMO Tech. Doc. 1073, 84 pp. [Available online at http://www.wmo.int/pages/prog/arep/gaw/documents/gaw143.pdf.]

——, 2007: WMO Global Atmosphere Watch (GAW) strategic plan: 2008–2015—A contribution to the implementation of the WMO strategic plan: 2008–2011. GAW Rep. 172/WMO Tech. Doc. 1384, 62 pp. [Available online at http://www.wmo.int/pages/prog/arep/gaw/documents/gaw172-26sept07.pdf.]

Zellweger, C., J. Forrer, P. Hofer, S. Nyeki, B. Schwarzenbach, E. Weingartner, M. Ammann, and U. Baltensperger, 2003: Partitioning of reactive nitrogen (NOy) and dependence on meteorological conditions in the lower free troposphere. *Atmos. Chem. Phys.,* **3,** 779–796.